

# Stroke

JOURNAL OF THE AMERICAN HEART ASSOCIATION

**Embolus trajectory through a physical replica of the major cerebral arteries**  
Emma M Chung, James P Hague, Marie-Anne Chanrion, Kumar V Ramnarine, Emmanuel  
Katsogridakis, and David H Evans  
STROKE/2009/574400 VERSION 1  
Article Type: Original Contributions

**This information is current as of November 28, 2009**

## **Author Disclosures**

**Emma M Chung:** No disclosures

**James P Hague:** No disclosures

**Marie-Anne Chanrion:** No disclosures

**Kumar V Ramnarine:** No disclosures

**Emmanuel Katsogridakis:** No disclosures

**David H Evans:** No disclosures

# **Embolus trajectory through a physical replica of the major cerebral arteries**

Emma M.L. Chung, PhD; James P. Hague, PhD, Marie-Anne Chanrion, BSc; Kumar V. Ramnarine, PhD; Emmanuel Katsogridakis, MD; David H. Evans, DSc.

From the University of Leicester Department of Cardiovascular Sciences, UK (E.M.L.C., E.K., D.H.E.), Open University Department of Physics and Astronomy, UK (J.P.H.); Université de Lyon, France (M-A.C.), and University Hospitals of Leicester NHS Trust, UK (K.V.R.).

**Correspondence:** Dr Emma Chung, Department of Cardiovascular Sciences, University of Leicester, Leicester Royal Infirmary, Leicester, LE1 5WW, UK.

**E-mail:** [emlc1@le.ac.uk](mailto:emlc1@le.ac.uk)

**Tel:** +44 116 2541414 ext 6065

**Fax:** +44 116 2586070

**Words:** 3566

**Acknowledgements**

This research was funded by the British Heart Foundation (FS/08/055/24297). We thank Professor Ronney Panerai for advice during implementation of the model.

**Disclosures**

No conflicts of interest.

# **Embolus trajectory through a physical replica of the major cerebral arteries**

**Cover title:** Embolus trajectory through the cerebral arteries

**Table 1** MS Word

**Fig 1** Color

**Fig 2** Grayscale

**Fig 3** Color

**Fig 4** Color

**Fig 5** Grayscale

**Subject codes:** [53] Embolic stroke, [59] Doppler ultrasound, Transcranial Doppler etc.

**Key Words:** Transcranial Doppler; embolic stroke; experimental; cerebral hemodynamics

## **Short abstract:**

This study investigates the motion of emboli microspheres through a physiologically realistic 3D replica of the cerebral macrocirculation. We found that embolus trajectory was dependent on embolus size and deviated significantly from expectations based on volume flow. Large emboli favored the middle cerebral artery, which is consistent with clinical observations.

**Abstract** (245/250 words)

**Background and Purpose**– The observed distribution of cerebral infarcts varies markedly from expectations based on blood-flow volume or Doppler embolus detection. In this study we use an *in vitro* model of the cerebral arteries to test whether embolus microspheres encountering the Circle of Willis are carried proportionally to volume flow, or express a preferred trajectory related to arterial morphology or embolus size.

**Methods**- Our model consisted of a patient-specific silicone replica of the cerebral macrocirculation featuring physiologically realistic pulsatile flow of a blood-mimicking fluid at ~1000 mL/min and an input pressure of ~150/70 mmHg. Particles of 200, 500 and 1000 $\mu$ m diameter with equivalent density to thrombus were introduced to the carotid arteries and counted on exiting the model outlets.

**Results**- The Middle Cerebral Arteries (MCAs) of the replica attracted a disproportionate number of emboli compared to the Anterior Cerebral Arteries (ACAs); 98 $\pm$ 3% of 1000 $\mu$ m and 93 $\pm$ 2% of 500 $\mu$ m emboli entered the MCA compared to 82 $\pm$ 5% of the flow. The observed distribution of large emboli was consistent with the ratio of MCA:ACA infarcts, ~95% of which occur in territories supplied by the MCA. With decreasing embolus size the distribution of emboli approaches that of the flow (~89% of 200 $\mu$ m emboli took the MCA).

**Conclusions**– Embolus trajectory through the cerebral arteries is dependent on embolus size and strongly favours the MCA for large emboli. The 70:30 ratio of MCA:ACA emboli observed by Doppler ultrasound is consistent with the trajectories of small emboli that tend to be asymptomatic.

## Introduction

Epidemiological evidence,<sup>1,2</sup> autopsy studies,<sup>3,4</sup> and the trajectories of ‘balloon emboli’ in patients undergoing cerebral angiography<sup>5</sup> suggest that emboli incident from the Common Carotid Artery (CCA) are more than 20 times as likely to come to rest in territories supplied by the middle cerebral artery (MCA) than the Anterior Cerebral Artery (ACA). However, *in vivo* transcranial Doppler (TCD) ultrasound insonation of the MCA-ACA junction performed by Wijman *et al.* found emboli to be only 2-3 times more likely to enter the MCA<sup>6</sup> suggesting that emboli are carried roughly proportionally to flow volume. Wijman *et al.* concluded that “*cerebral embolism is unlikely to be the only cause of ACA and MCA infarcts*”. In this study we clarify the relationship between blood-flow, arterial topology, and embolisation by implementing a physiologically realistic 3D phantom of the major cerebral arteries to investigate embolus trajectory. We hope that a better understanding of the relationship between arterial topology, blood-flow, and embolus trajectory will assist in the development of patient-specific computer simulations for monitoring patients at high risk of stroke.<sup>7</sup> Although previous models of the Circle of Willis have been developed to investigate blood-flow,<sup>8-11</sup> ours is the first to use a 3D *in vitro* model of the cerebral arteries to study embolisation.

## Materials and methods

### Replica anatomy

A physical model of the cerebral arteries was purchased from a company specializing in vascular replicas (Elastrat, Geneva, Switzerland). Details of the data acquisition, post-processing, and model preparation performed by Elastrat are described by Wetzel *et al.*<sup>12</sup> The final physical replica consisted of left and right Vertebral Artery (VA) and CCA inlets, with pairs of outlets for the External Carotid Artery (ECA), Posterior Cerebral Artery (PCA), MCA and ACA. The phantom was made from a silicone elastomer with ~1 mm wall thickness, attenuation coefficient for ultrasound of 3.5 dB cm<sup>-1</sup> MHz<sup>-1</sup>, speed of sound of 1020 ms<sup>-1</sup>, and Young's elastic modulus of ~ 1.3 MPa.<sup>13</sup> The internal diameter of each vessel was measured from an enlarged B-mode image by calliper placement to an uncertainty of ≤ 0.5 mm. Vessel diameters are compared to average values in Table 1.

### Replica implementation

Inlet flows were generated by combining a pair of programmable gear pumps (Micropump model 120-000-1100, Concord, CA, USA) to produce a pulsatile waveform, as shown in Fig. 1(d). The circuit was completed using C-flex tubing (Cole Parmer, London, UK) and filled with a solution of 40% (by weight) glycerol in water ( $\rho=1099$  kg/m<sup>3</sup>,  $\mu=3.7$  mPa.s at 20°C). This water-glycerol solution possesses a similar density ( $\rho$ ) and viscosity ( $\mu$ ) to human blood ( $\rho=1053$  kg/m<sup>3</sup>,  $\mu=3$  mPa.s). For ultrasound insonation this fluid was replaced by a validated blood-mimicking fluid (BMF) containing Orgasol<sup>®</sup> particles to mimic the blood's acoustic scattering properties (BMF:  $\rho=1037$  kg/m<sup>3</sup>,  $\mu=4.1$  mPa.s).<sup>14</sup>

Pump settings were adjusted to achieve an overall flow rate through the model of ~1000 ml/min. Resistances were controlled by adjusting the lengths and diameters of C-flex tubing at the model inlets and outlets until flow rates were similar to those quoted by Scheel

*et al.*<sup>15</sup> totalling 328±111 ml/min for the ECAs (310 ml/min replica), 499±108 ml/min ICAs (517 ml/min replica) and 158±48 for the VAs (188 ml/min replica). The 3D phantom is reduced to a 2D representation of lengths and diameters in Fig. 2. The pressure waveform at the model inlets was recorded using a catheter equipped with a calibrated solid-state strain-gauge [Gaeltec, Isle of Skye, UK] and finometer [Finapres Medical Systems, BV, Amsterdam, NL]. Pulsatile flow at a rate of 1 ‘cardiac cycle’ per second was associated with a pressure of 150/70 mmHg.

Flow rates were measured by timed collection of fluid from the model outlets (Table 1). Dye injection and Doppler ultrasound measurements confirmed that the posterior arteries were supplied primarily by the VAs, while MCAs were mainly supplied by the ipsilateral CCA, Fig. 3. Velocity profiles in each of the major vessels were investigated using Doppler, Color flow, and B-mode ultrasound (z.one, Zonare, CA, US). Care was taken to ensure that the Doppler sample length was set to encompass the entire vessel lumen, and that velocities were angle-corrected with an angle of insonation of <60°. Since volume flow estimates based on the intensity-weighted time-averaged mean velocity (TAMV) are associated with significant errors<sup>16</sup> we also performed physical measurements of emboli and flow-rates by timed collection from the replica outlets. Reynolds numbers were estimated for each of the major arteries and ranged between 100 and 600, which is consistent with laminar flow in a straight tube.

### **Investigation of embolus trajectory**

Embolus trajectories were investigated for three sizes of colored microspheres with mean diameters of 200 µm (black), 500 µm (red), and 1000 µm (white) (Duke Scientific, CA, US). The spheres were fabricated from cross-linked polystyrene divinylbenzene with a density of

$\rho_{spheres}=1050 \text{ kg/m}^3$ . These spheres have a similar density to thrombus ( $\rho_{thrombus}\sim 1060 \text{ kg/m}^3$ ), and provided model emboli that were approximately neutrally buoyant.

A mixed suspension of 200, 500 and 1000  $\mu\text{m}$  microspheres was gradually introduced to the CCAs of the replica using a 10 ml syringe. Particles were injected simultaneously to ensure that all sizes experienced identical flow conditions. Differences in embolus trajectory could therefore be attributed exclusively to the impact of embolus size rather than fluctuations in flow conditions. Emboli were packed into the syringe as densely as possible to minimise the volume of fluid added to the system during injection (<10 ml over 2 mins) and the model was flushed between injections to remove any stray microspheres. A qualitative insight into embolus trajectory was gained by imaging the circle of Willis using a high-speed digital camera operating at 300 frames per second (EXILIM Pro EX-F1, Casio, Tokyo, Japan).

Corresponding volume flow measurements were obtained by weighing the quantity of fluid in each of the reservoirs after 2 mins of timed collection. A total of  $N=1273$  (1000  $\mu\text{m}$ ),  $N=6300$  (500  $\mu\text{m}$ ), and  $N=1757$  (200  $\mu\text{m}$ ) emboli were introduced to the model over several injections. Emboli exiting the model outlets were retrieved using a 38  $\mu\text{m}$  fine-mesh filter and counted from an enlarged image of the filter's contents to determine the average number of emboli from each vessel, Fig. 1(b).

To test the hypothesis that emboli are distributed proportionally to volume flow, we defined our null hypothesis as the distribution expected assuming a uniform concentration of emboli throughout the fluid (irrespective of embolus size or arterial topology). Experimental data were compared to the null hypothesis using a  $\chi^2$  Goodness of Fit test (Statistica v. 5.1, Tulsa, USA).

## Results

Inspection of video footage (supplemental movie 1) showed that the left ACA (A2 segment) was partially supplied by the right ACA throughout the cardiac cycle, with a small (clockwise) crossover of flow between anterior and posterior circulations at peak systole. Filling of distal ACA segments from the contralateral side is a common clinical finding<sup>6,17,18</sup> reflecting the patient-specific nature of our replica. An asymmetry in flows occurs because the diameter of the left ACA A1 segment is ~1 mm less than on the right side producing a higher resistance. Arteries in which emboli were found were consistent with this slight asymmetry in the flow distribution identified by dye injection.

Results from injecting a mixture of 500  $\mu\text{m}$  and 1000  $\mu\text{m}$  diameter spheres to (a) the left and (b) the right CCAs during pulsatile flow are presented in Fig. 4. We found that remarkably few 1000  $\mu\text{m}$  emboli entered the ACAs, and concentrations of emboli in the ACA were much lower than elsewhere. When high-speed video of emboli moving past the Circle of Willis was slowed to 30 fps (equivalent to 1 cardiac cycle every 10 seconds) the preference of large emboli for the MCA could be clearly observed, supplemental movie 2. Simultaneous bilateral injection of 200, 500 and 1000  $\mu\text{m}$  microspheres revealed that the distribution of emboli tended toward that of the flow with decreasing embolus size, Fig. 4 (c). For the smallest 200  $\mu\text{m}$  spheres, the distribution of particles was within 3% of the flow distribution.

Assuming emboli are distributed proportionally to flow volume, the normalised concentration of particles is expected to remain constant (equal to 1) throughout the replica. Embolus concentrations in the fluid shown in Fig. 5 demonstrated a marked decrease in embolus concentration in ACA and ECA branches compared to the ICA and MCA (particularly with increasing embolus size). In fact, the average concentration of 1000  $\mu\text{m}$  emboli in the MCA was over ten times higher than in the ACA. Results for 1000  $\mu\text{m}$  and 500

$\mu\text{m}$  emboli clearly show significant deviations from the null hypothesis distribution. A  $\chi^2$  Goodness of Fit test rejected the null hypothesis to a level of significance of  $p < 0.001$  for 1000  $\mu\text{m}$  and 500  $\mu\text{m}$  emboli, and  $p = 0.017$  for 200  $\mu\text{m}$  emboli.

## Discussion

This study investigated the motion of emboli with a similar density to thrombus through a patient-specific replica of the major cerebral arteries under physiologically realistic pulsatile flow conditions. Large emboli were found to adopt a preferred trajectory through the arteries, which approaches the volume flow distribution with decreasing embolus size. The hypothesis that emboli are distributed proportionally to flow volume was rejected to a high level of significance for 500  $\mu\text{m}$  and 1000  $\mu\text{m}$  emboli ( $p < 0.001$ ), and to a level of  $p = 0.017$  for 200  $\mu\text{m}$  emboli, based on comparison with our data using a simple  $\chi^2$  test.

The preferred trajectory of emboli produced a concentration of 1000  $\mu\text{m}$  emboli in the MCA that was over ten times higher than in the ACA. At the MCA-ACA junction, 93-98% of 500-1000  $\mu\text{m}$  emboli entered the MCA compared to 82% of the flow. This preference of large emboli to enter the MCA is consistent with the high ratio of MCA:ACA infarcts (~95%) reported by the Harvard<sup>1</sup> and Lausanne<sup>2</sup> stroke registry studies. A 95:5 ratio of MCA:ACA infarction is considerably higher than would be expected if emboli were carried proportionally to flow volume. Reference data published by Tanaka *et al.* suggests the a ratio of MCA to ACA flow of approximately 75:25,<sup>19</sup> which is similar to the 70:30 ratio of MCA:ACA emboli detected by Doppler ultrasound.<sup>6</sup> The discrepancy between the distribution of cerebral infarcts and Doppler embolic signals was thought by Wijman *et al.*<sup>6</sup> to suggest that emboli cannot be the only cause of cerebral infarcts. However, as Doppler ultrasound is capable of detecting small particles (>100  $\mu\text{m}$ ) and even smaller gas bubbles (>4  $\mu\text{m}$ ), and does not give an estimate of embolus size, it is more likely that the majority of

emboli detected by TCD are asymptomatic and distributed proportionally to the flow due to their small size. In our replica, the MCAs received ~82% of the flow, while the number of emboli varied from 98% (1000  $\mu\text{m}$ ) to 89% (200  $\mu\text{m}$ ) with decreasing embolus size. This preferred trajectory of these emboli is consistent with large emboli being the primary cause of ACA and MCA infarcts. We therefore conclude that no additional mechanism of cerebral infarction needs to be taken into account in addition to embolism.

The tendency for tiny emboli to be distributed proportionally to blood flow is consistent with the trajectories of small particles (e.g. red-blood aggregates) which are assumed to be carried homogeneously within the flow for large vessels. Our results are also consistent with expectations based on previous *in vitro* fluid dynamics studies of isolated bifurcations. Pollanen and co-workers investigated vessels with side branches and found that emboli with diameters  $>200 \mu\text{m}$  preferred to follow the path of the trunk vessel.<sup>20,21</sup> In Y-shaped bifurcations studied by Bushi *et al.* larger emboli were also found to exhibit a preference for wider branches.<sup>22</sup> Hemodynamics in the circle of Willis have been studied in glass models by Roach *et al.*<sup>23</sup>, and are the focus of a number of theoretical studies.<sup>24-28</sup> However, we could find no reports of computational modelling of embolus trajectory.

A limitation of our study is that we only examined a single composition of embolus with an equivalent density to thrombus; the distributions of gas or fat emboli may differ significantly from the distribution reported here. The presence of a significant carotid stenosis also has potential to alter the distribution of emboli by introducing turbulence. However, turbulence dissipates rapidly in the post-stenotic region and is likely to have disappeared by the time the blood flow reaches the circle of Willis.<sup>29</sup> The fundamental finding of a variation in embolus trajectory with embolus size is unlikely to be unaffected by variations in arterial topology or pathology.

In our anatomical replica, small branches (such as the pontine, lateral striate, and ophthalmic arteries) were absent. Although, ultrasound measurements of vessel diameters and flow velocities are affected by reflection, refraction and attenuation effects produced by differences in acoustic properties of the blood mimic, vessel wall elastomer, and surrounding water,<sup>30,31</sup> these factors do not alter our final conclusions which are based on physical counting of emboli.

### **Conclusions**

Large emboli travel a preferred trajectory through the cerebral arteries which strongly favours the MCA over the ACA in excess of expectations based on differences in blood flow volume. Our results for large emboli produce a similar distribution as found in stroke patients, with a >95% rate of embolism in MCA territories. Smaller emboli are carried proportionally to flow volume, explaining the apparent discrepancy between embolus trajectories observed using transcranial Doppler and the distribution of cerebral infarctions.

## References

- [1] Mohr JP, Caplan LR, Melski JW, Goldstein RJ, Duncan GW, Kistler JP, Pessin MS, Bleich HL. The Harvard cooperative stroke registry: a prospective registry. *Neurology*. 1978;28:754-62.
- [2] Bogousslavsky J, Regli F. Anterior cerebral artery territory infarction in the Lausanne stroke registry. *Arch Neurol*. 1990;47:144-150.
- [3] Masuda J, Yutani C, Ogata J, Kuriyama Y, Yamaguchi T. Atheromatous embolism in the brain: a clinicopathologic analysis of 15 autopsy cases. *Neurology*. 1994;44:1231-1237.
- [4] Torvik A, Skullerud K. Watershed infarcts in the brain caused by microemboli. *Clin Neuropathol*. 1982;1:99-105.
- [5] Gacs GY, Merei FT, Bodosi M. Balloon catheter as a model of cerebral emboli in humans. *Stroke*. 1982;13:39-42.
- [6] Wijman CAC, Babikian VL, Winter MR, Pochay VE. Distribution of cerebral microembolism in the anterior and middle cerebral arteries. *Acta Neurol Scand*. 2000;101:122-127.
- [7] Chung EML, Hague JP and Evans DH. Revealing the mechanisms underlying embolic stroke using computational modelling. *Phys Med Biol*. 2007;52:7153-7166.
- [8] Avman N, Bering EA. A plastic model for the study of pressure changes in the circle of Willis and major cerebral arteries following arterial occlusion. *J Neurosurg*. 1961;18:361-365.
- [9] Rogers L. The function of the circulus arteriosus of Willis. *Brain*. 1947;70:171-178.
- [10] Cieslicki K, Ciesla D. Investigations of flow and pressure distributions in physical model of the circle of Willis. *J Biomech*. 2005;38:2302-10.
- [11] Fasano VA, Portalupi A, Broggi G. Study of cerebral hemodynamics by analogic models. *Vasc Dis*. 1966;3:89-99.
- [12] Wetzel SG, Makoto O, Handa A, Auer J-M, Lylyk P, Lovblad K-O, Babic D, Rufenacht DA. From patient to model: stereolithographic modelling of the cerebral vasculature based on rotational angiography. *AJNR Am J Neuroradiol*. 2005;26:1425-1427.
- [13] Poepping T, Nikolov HN, Thorne M, Holdsworth DW. A thin-walled carotid vessel phantom for ultrasound flow studies. *Ultrasound Med Biol*. 2004;30:1067-1078.
- [14] Ramnarine KV, Nassiri DK, Hoskins PR, Lubbers J. Validation of a new blood-mimicking fluid for use in Doppler flow test objects. *Ultrasound Med Biol*. 1997;24:451-459.
- [15] Scheel P, Ruge C, Petruch UR, Schoning M. Color duplex measurement of cerebral blood flow volume in healthy adults. *Stroke*. 2000;31:147-150.
- [16] DH Evans and WN McDicken. *Doppler Ultrasound: Physics, Instrumentation and signal processing*. 2nd Edition. Wiley, Chichester, UK. 2000.
- [17] Babikian VL, Wechler LR (eds). *Transcranial Doppler ultrasonography*. Boston, MA: Butterworth Heinemann. 1999.

- [18] Kansagra AP, Wong EC. Quantitative assessment of mixed cerebral vascular territory supply with vessel encoded arterial spin labelling MRI. *Stroke*. 2008;39:2980-2985.
- [19] Tanaka H, Fujita N, Enoki T, Matsumoto K, Watanabe Y, Murase K, Nakamura H. Relationship between variations in the circle of Willis and flow rates in internal carotid and basilar arteries determined by means of magnetic resonance imaging with semiautomated lumen segmentation: reference data from 125 healthy volunteers. *AJNR Am J Neuroradiol*. 2006;27:1770-1775.
- [20] Pollanen MS, Deck JH. The mechanism of embolic watershed infarction: experimental studies. *Can J Neurol Sci*. 1990;17:395-398.
- [21] Pollanen MS. Behavior of suspended particles at bifurcations: implications for embolism. *Phys Med Biol*. 1990;36:397-401.
- [22] Bushi D, Grad Y, Einav S, Yodfat O, Nishri B, Tanne D. Hemodynamic evaluation of embolic trajectory in an arterial bifurcation. *Stroke*. 2005;36:2696-2700.
- [23] Roach MR, Scott S, Ferguson GG. The hemodynamic importance of the geometry of bifurcations in the circle of Willis (Glass model studies). *Stroke*. 1972;3:255-267.
- [24] Alastruey J, Parker KH, Peiró J Byrd SM, Sherwin SJ. Modelling the circle of Willis to assess the effects of anatomical variations and occlusions on cerebral flows. *J Biomech*. 2007;40:1794-1805.
- [25] Cassot F, Vergeur V, Bossuet P, Hillen B, Zagzoule M, Marc-vergnes J-P. Effects of anterior communicating artery diameter on cerebral hemodynamics in internal carotid artery disease: a model study. *Circulation*. 1995;92:3122-3131.
- [26] Grinberg L, Anor T, Madsen JR, Yakhot A, Karniadakis GE. Large-scale simulation of the human arterial tree. *Clin Exp Pharmacol Physiol*. 2009;36:194-205.
- [27] Cebra JR, Castro MA, Soto O, Löhner R, Alperin N. Blood-flow models of the circle of Willis from magnetic resonance data. *J Eng Math*. 2003;47:369-386.
- [28] Moore S, David T, Chase JG, Arnold J and Fink J. 3D models of blood flow in the cerebral vasculature. *Journal of Biomechanics*. 2006;39:1454-1463.
- [29] Long Q, Xu XY, Ramnarine KV, Hoskins PR. Numerical investigation of physiologically realistic pulsatile flow through arterial stenosis. *Journal of Biomechanics*. 2001;34:1229-1242.
- [30] Christopher DA, Burns PN, Hunt JW and Foster FS. The effect of refraction and assumed speeds of sound in tissue and blood on Doppler ultrasound blood velocity-measurements. *Ultrasound Med Biol*. 1995;21:187-201.
- [31] Hoskins PR and Ramnarine KV. Doppler Test Devices. In: *Doppler Ultrasound: Physics, Instrumentation and signal processing*. 2nd Edition. DH Evans and WN McDicken. Wiley, Chichester, UK. 2000.

## Figures

**Fig. 1.** (a) Overview of the experimental apparatus. (b) Microspheres were retrieved from the model outlets using a 38  $\mu\text{m}$  sieve. (c) Microspheres moving past the circle of Willis after right CCA injection (see supplemental movie file 2). (d) Input pressure waveform.

**Fig. 2.** Phantom dimensions reduced to a 2D schematic. Vessel segment lengths in cm are followed by internal diameters in brackets.

**Fig. 3.** Replica during dye injection to the Right CCA (red), left CCA (green) and posterior circulation (yellow). For dynamic properties during pulsatile flow please view supplemental movie file 1. Note that the left ACA A2 is partially supplied by the contralateral side due to narrowing in the left ACA A1 segment. Examples of Doppler spectra measuring flow profiles in the ICA, MCA and ACA (A1 and A2) segments are also shown.

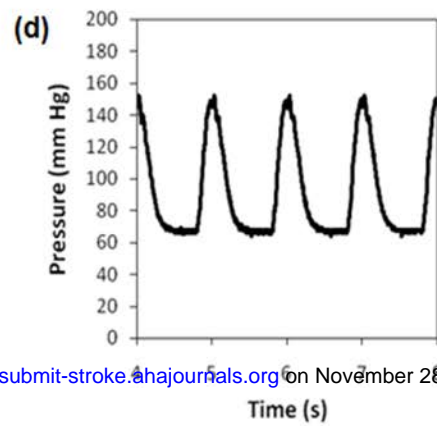
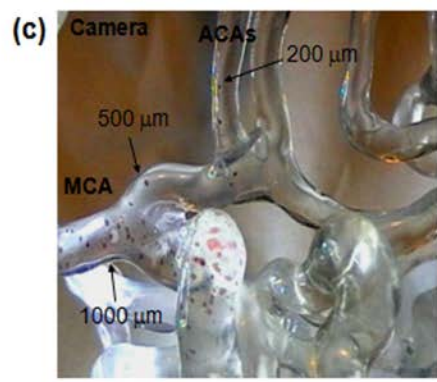
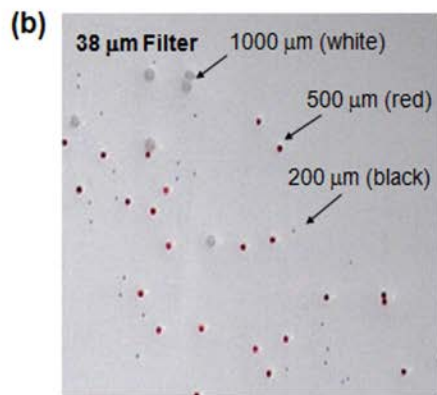
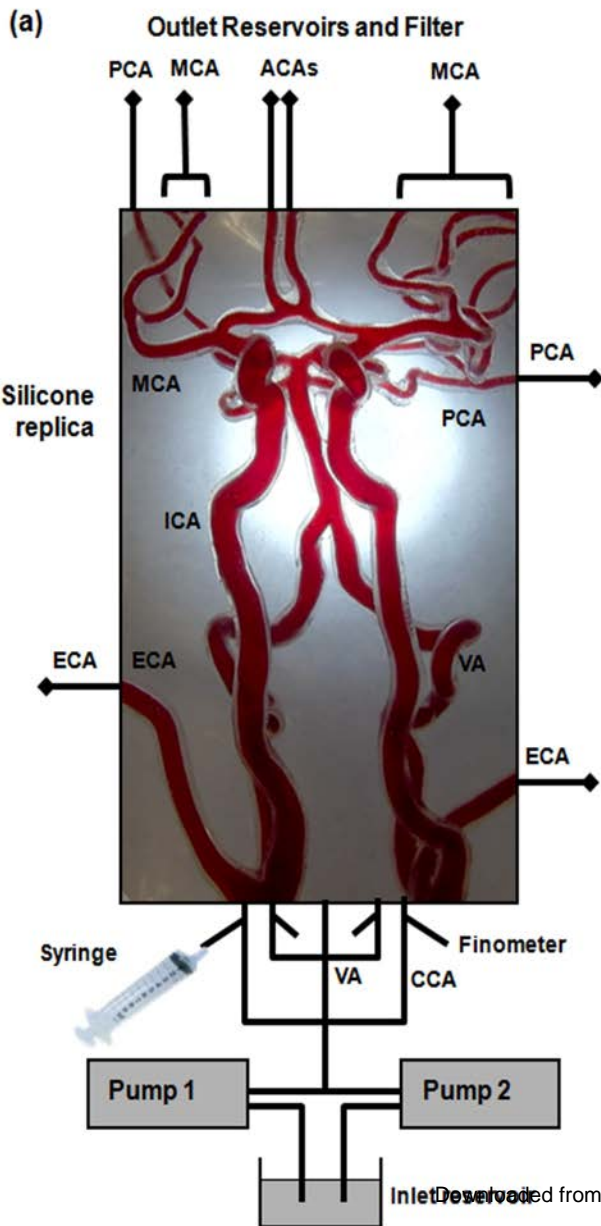
**Fig. 4.** Comparison of percentage volume flow and percentage of 500  $\mu\text{m}$  (red) and 1000  $\mu\text{m}$  (white) emboli retrieved from each of the outlets after (a) right and (b) left CCA injection. More emboli entered the MCA than would be expected based on volume flow. (c) Bilateral injection to the CCAs of 200  $\mu\text{m}$  (black), 500  $\mu\text{m}$  and 1000  $\mu\text{m}$  emboli showed the distribution of smaller emboli to approach that of the flow.

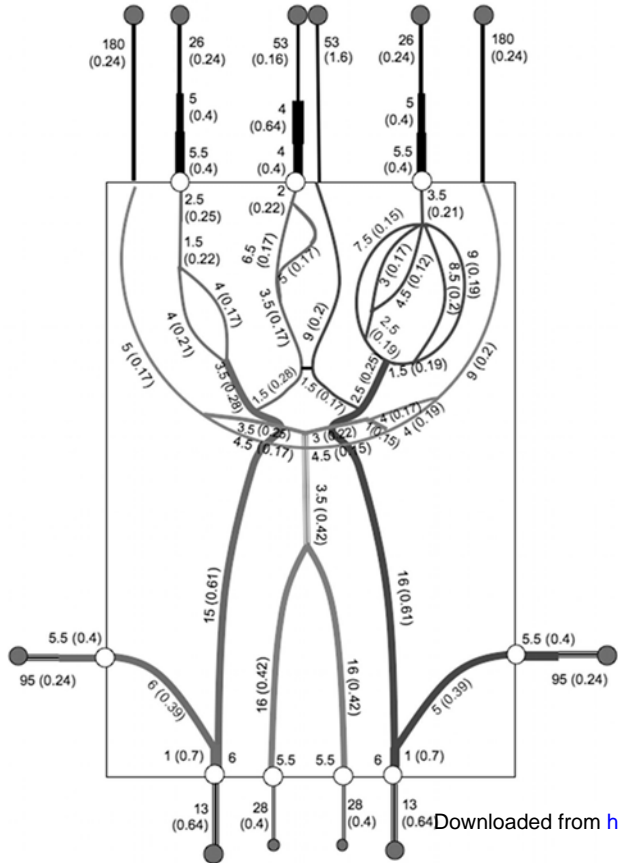
**Fig. 5.** Concentrations of emboli measured relative to the CCA were lower in the ACA and ECA than in the MCA and ICA. Lines provide a guide to the eye. The null hypothesis, representing no change in embolus concentration with flow ratio, corresponds to the horizontal line (equal to 1). Deviations from the null hypothesis increase with embolus size.

## Table

**Table 1. Dimensions and volume fluid flow through the replica.**

Artery	Diameter (cm)		Flow volume (mL/min)	
	Replica ( $\pm 0.05$ cm)	Clinical average <sup>26</sup>	Outlet flow ( $\pm 4\%$ )	Doppler ( $\pm 32\%$ )
RCCA	0.61	0.5	410	401
LCCA	0.61		417	384
RECA	0.39	0.3	159	153
LECA	0.39		151	154
RICA	0.61	0.4		374
LICA	0.61			401
RMCA	0.28	0.29	223	195
LMCA	0.25		228	201
RACA-A1	0.28	0.23		53
LACA-A1	0.17			29
RACA-A2	0.17	0.24	28	29
LACA-A2	0.2		38	29
RPCA	0.22	0.21	79	72
LPCA	0.25		73	76
BA	0.42	0.32		120
RVA	0.42	0.27		101
LVA	0.42			87
<b>Total flow</b>			<b>979</b>	<b>1082</b>

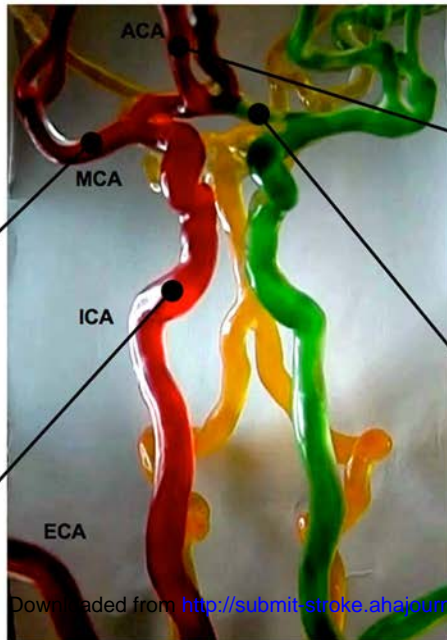
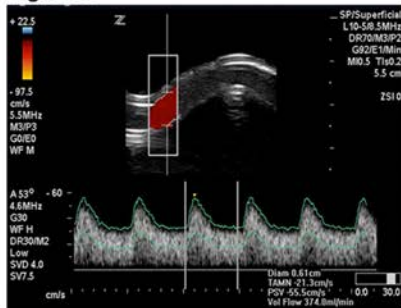




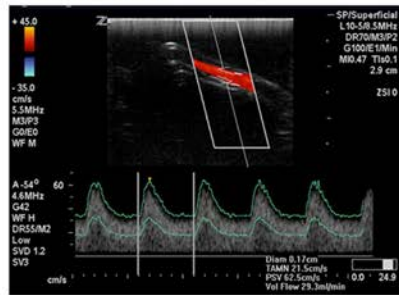
## Right MCA



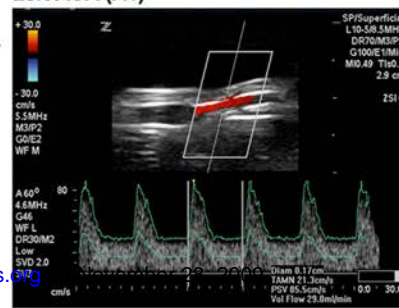
## Right ICA



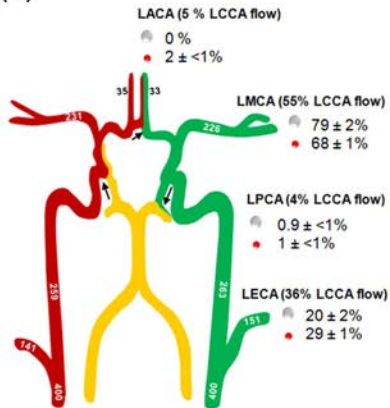
## Right ACA (A2)



## Left ACA (A1)

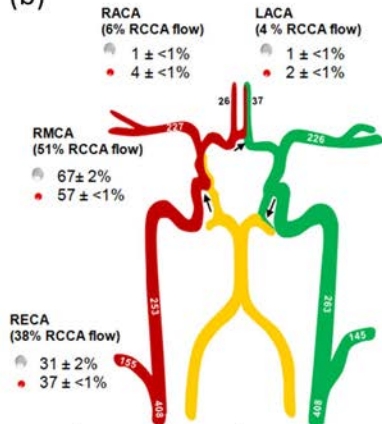


(a)

**LCCA Injection**

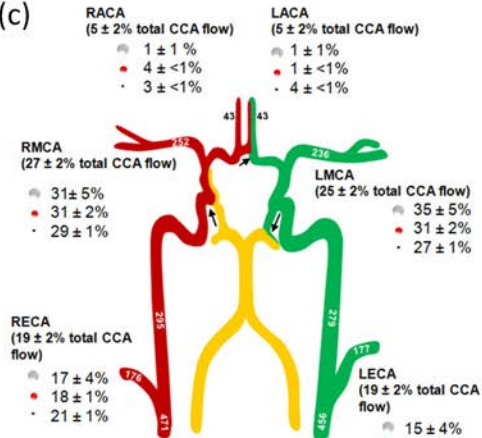
- N=465 (1000 μm)
- N=2067 (500 μm)

(b)

**RCCA Injection**

- N=705 (1000 μm)
- N=3454 (500 μm)

(c)

**Bilateral CCA Injection**

- N=103 (1000 μm)
- N=799 (500 μm)
- N=1757 (200 μm)

